NANO LETTERS

pubs.acs.org/NanoLett Letter

Liposome Imaging in Optically Cleared Tissues

Abdullah Muhammad Syed,[○] Presley MacMillan,[○] Jessica Ngai,[○] Stefan Wilhelm, Shrey Sindhwani, Benjamin R. Kingston, Jamie L. Y. Wu, Pablo Llano-Suárez, Zachary Pengju Lin, Ben Ouyang, Zaina Kahiel, Suresh Gadde, and Warren C. W. Chan*

Cite This: *Nano Lett.* 2020, 20, 1362−1369 Read Online

ABSTRACT: Three-dimensional (3D) optical microscopy can be used to understand and improve the delivery of nanomedicine. However, this approach cannot be performed for analyzing liposomes in tissues because the processing step to make tissues transparent for imaging typically removes the lipids. Here, we developed a tag, termed REMNANT, that enables 3D imaging of organic materials in biological tissues. We demonstrated the utility of this tag for the 3D mapping of liposomes in intact tissues. We also showed that the tag is able to monitor the release of entrapped therapeutic agents. We found that liposomes release their cargo >100-fold faster in tissues *in vivo* than in conventional *in vitro* assays. This allowed us to design a liposomal formulation with enhanced ability to kill tumor associated macrophages. Our development opens up new opportunities for studying the chemical properties and pharmacodynamics of administered organic materials in an intact biological environment. This approach provides insight into the *in vivo* behavior of degradable materials, where the newly discovered information can guide the engineering of the next generation of imaging and therapeutic agents.

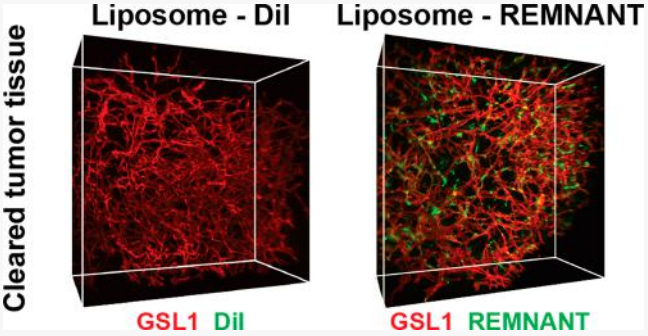

KEYWORDS: *Nanoparticles, CLARITY, 3D imaging, fluorescent label, tissue clearing*

Efficient delivery of nanoparticles to tumors is a key challenge for the translation of nanoparticles for cancer therapy. This challenge has remained unaddressed so far because the transport and distribution of nanoparticles within the tumor is not completely understood.[1−3] The key parts of this process are that nanoparticles enter the tumor through blood vessels, get transported through the tumor matrix and then captured by cancer cells and immune cells in the tumor, or escape the tumor through lymphatic vessels.[4,5] These key processes cannot be directly observed in a tumor because tissues are opaque, and because of this, optical microscopy only allows visualization up to approximately 50 μm deep into the tissue. To visualize blood and lymphatic vessels deep inside the tissue, the tissue needs to be rendered transparent.[6−10]

We have recently developed methods for making tissues transparent to enable 3D microscopy of inorganic nanoparticles in the tumor. Our key finding was that inorganic nanoparticles could be retained and visualized as long as they were intrinsically fluorescent (such as quantum dots)[11,12] or possessed strong intrinsic light scattering (such as gold nanoparticles).[13] We have started to apply these approaches to understand the distribution of inorganic nanoparticles in tumors based on key features that can only be visualized in 3D, such as the blood vessel structure.[14] However, we were unable to visualize organic nanoparticles, namely, liposomes and polymer nanoparticles.

Mapping the distribution of lipid-based nanoparticles in 3D is an unaddressed challenge. This is important because nearly all currently approved nanoparticle formulations are lipid nanoparticles. Lipid nanoparticles offer substantial advantages in synthesis, encapsulation, and biocompatibility.[15] However, the typical procedure to make tissues transparent for 3D microscopy removes or disrupts the lipid membranes to minimize the optical scattering of the tissue.[6,16,17] Optical scattering is the key factor that makes tissues opaque, and the elimination of optical scattering makes tissues transparent.[18] This is typically achieved by first cross-linking primary amine groups on the proteins to preserve the protein structure. Then, strong detergents or organic solvents are used to disrupt and remove lipid membranes in the tissue.[6,7,16,17,19] Lipids typically lack primary amine groups, so they are not protected by the previous cross-linking step. Once lipids are removed, key proteins are fluorescently labeled to visualize the structure of the original tissue when the tumor was alive.

Received: November 22, 2019
Revised: December 23, 2019
Published: January 13, 2020

https://dx.doi.org/10.1021/acs.nanolett.9b04853
Nano Lett. 2020, 20, 1362−1369

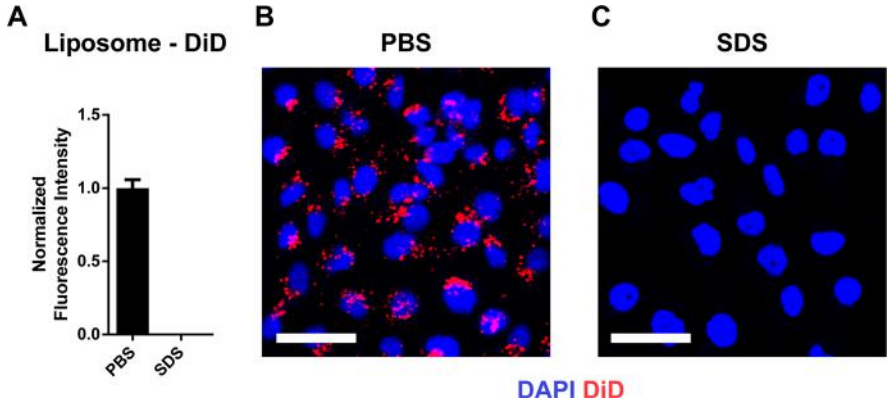

Figure 1. Liposome DiD signals inside cells are lost when cells are treated with SDS. MDA-MB-231 cells were treated with DiD-labeled liposomes and fixed and cross-linked using the CLARITY protocol. They were then treated with phosphate-buffered saline (PBS, 1×) or sodium dodecyl sulfate (SDS, 4%). (A) Quantification of DiD fluorescence retained in the cells with PBS or SDS treatment. Confocal microscope image of cells treated with PBS (B) or SDS (C). Scale bar indicates 50 μm.

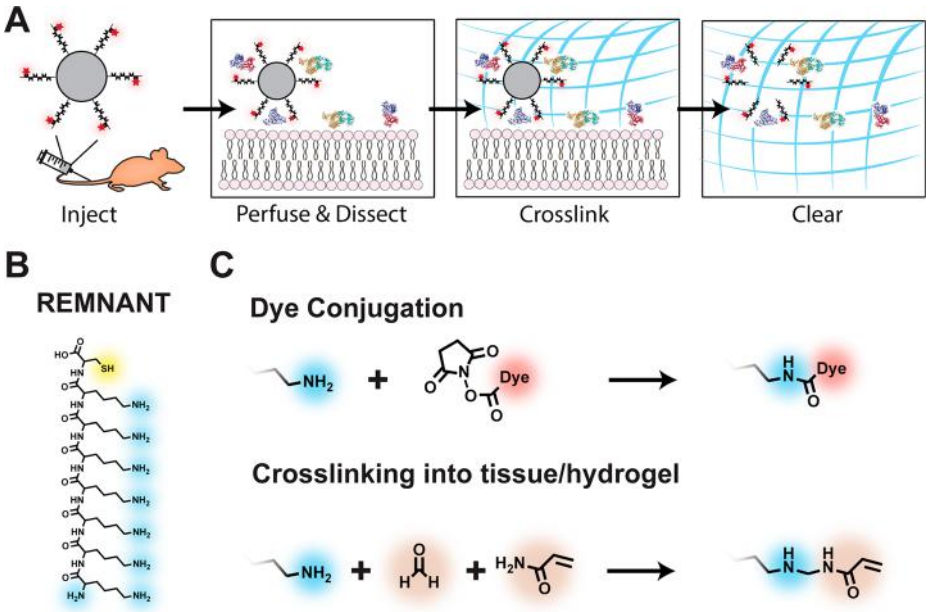

Figure 2. REMNANT contains multiple amine groups enabling simultaneous fluorescent labeling and cross-linking. (A) Materials conjugated with the peptide tag can be injected into an animal, perfused, and dissected. The tag becomes cross-linked along with tissue proteins. The clearing process removes lipids, but the cross-linked proteins and tags are retained even when the nanoparticle is removed. (B) Structure of REMNANT peptide with sequence KKKKKKKC (K_7C). (C) Possible reactions for the amine groups within the peptide tag. Each amine group can undergo no reaction, a dye conjugation reaction before injecting into an animal, or a cross-linking reaction in the tissue.

This approach does not allow us to visualize the distribution of lipid nanoparticles.[20] To solve this problem, we propose the use of cross-linkable tags for the liposomes. These tags are attached to the surface of liposomes prior to injection into an animal. While the animal is alive, the tags remain attached to the liposome but when the tissue is treated with fixatives they become cross linked into the tissue. This cross linking allows the final distribution of the liposomes to be visualized.

■ RESULTS

We first examined whether we could observe liposomes after treatment with individual reagents commonly used for tissue clearing. Since we are interested in the effect of the reagents on liposomes, we tested this *in vitro* because a single layer of cells is transparent in all of these solutions. We prepared liposomes with the same lipid composition as Doxil. We fluorescently labeled these liposomes with a fluorescent lipid dye (DiD) and incubated them with MDA-MB-231 cells. We fixed and cross-linked these cells using formaldehyde and acrylamide to preserve the protein architecture. We incubated some cells with 4% sodium dodecyl sulfate (SDS) to render them transparent while other cells were incubated with phosphate-buffered saline (PBS) as a control. Relative to the control, we found that 99% of the fluorescent signal was lost after incubation with SDS (see Figure 1A−C). This confirmed that liposomes are currently not suitable for imaging in tissues cleared with SDS.

To overcome this problem, we explored the use of a fluorescent tag that could be attached to the liposome but would be cross-linked into the tissue and retained when lipids in the tissue are removed (Figure 2A). The key requirement for this tag is to have 3 covalently linked components: (1) a fluorescent label, (2) multiple free amine groups, and (3) an

https://dx.doi.org/10.1021/acs.nanolett.9b04853
Nano Lett. 2020, 20, 1362−1369

orthogonal functional group to conjugate the tag to the nanoparticle. Multiple amine groups are needed because some will be used to attach fluorescent dyes covalently. Out of the remaining, the cross-linking step only cross-links a small fraction into the tissue. We designed an amino acid tag termed REMNANT (REtained Molecular NANoparticle Tag) containing one cysteine and seven lysine groups (Figure 2B). Each amine on this tag is able to undergo either dye conjugation or tissue cross-linking reactions (Figure 2C). An important feature of REMNANT is that the same molecule participates in both reactions so that the fluorophore ends up covalently conjugated to the tissue. After cross-linking, the tag will mark the position of the liposomes within cleared tissues.

To accomplish this, we first synthesized azide functionalized liposomes by incorporating 2% mol/mol of an azide containing lipid (DSPE-PEG-Azide) into our lipid mixture prior to drying and extruding. By utilizing copper-free click chemistry, we were able to conjugate REMNANT and Cy5-NHS dye to our liposomes using an intermediate dibenzocyclooctyne maleimide (DBCO-Mal), resulting in stable REMNANT-labeled liposomes (Table S1).

We first tested REMNANT-labeled liposomes *in vitro* to validate and quantify its fluorophore retention (Figure S1). Both REMNANT- and DiO-labeled liposomes were incubated with RAW264.7 murine macrophage cells. Cells were cross-linked and cleared prior to imaging with confocal microscopy. The fluorescent signal from each sample was obtained, and the signal intensity was analyzed. As shown in Figure S1, the addition of the REMNANT label to the surface of the liposomes resulted in the retention of more than 50% of the fluorescent signal after treatment with SDS solution. We expect some loss of fluorescence because only a small fraction of amine groups are cross-linked to the hydrogel so that many REMNANT molecules will not be cross-linked. In contrast, labeling liposomes with only a lipophilic dye, DiO, resulted in a 99% loss of fluorescent signal after SDS treatment (Figure 1A, Figure S1).

We next confirmed that the REMNANT signal could be observed in cleared tissues and used to track liposome distribution. Liposomes labeled with REMNANT-Cy3 were intravenously administered to CD1-nude mice with U87MG xenograft tumors and allowed to circulate for 24 h. Blood vessels were labeled with GSLI-Cy5, mice were perfused and tissues cleared using the CLARITY, 3DISCO, and CUBIC protocols as these are the most commonly used tissue clearing methods.[6,7,16] 3D images of the cleared tissues were obtained using a Leica SP8 confocal microscope. Across all three tissue clearing methods, liposomes labeled with DiI, a fluorescent lipid dye, could not be visualized, but those labeled with REMNANT retained the fluorescent signal in the cleared tissues (Figure 3).

We also tried to visualize another organic nanoparticle, poly(lactic-*co*-glycolic acid) (PLGA) nanoparticles, using REMNANT because they are another widely used and clinically tested formulation. We were able to visualize the REMNANT signal in tumors from PLGA-REMNANT nanoparticles (Figure S2).

We realize that the tag could affect the surface charge of the nanoparticle because the amine groups are positively charged. This has the potential to change the transport and distribution of nanoparticles. We verified that the ζ potentials of liposomes were made with and without REMNANT, and we found that they were similar (5.48 mV vs 2.72 mV, respectively). It was

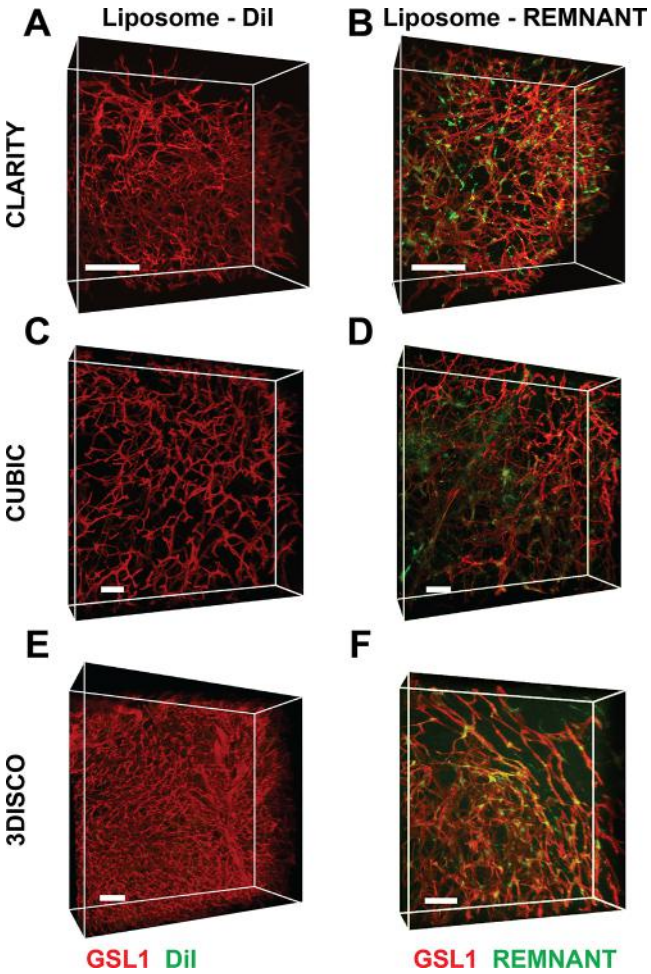

Figure 3. 3D maximum intensity projections of tumors containing liposome DiI (A, C, E) or liposome REMNANT (B, D, F). All images show blood vessels labeled with GSL1 in red and liposomes in green. Scale bars indicate 150 μm.

important for us to verify that the tag does not change the tissue-level distribution within the tumor because the key purpose of the tag is to map the distribution of the nanoparticle. The challenge with directly characterizing this distribution is that lipid nanoparticles cannot be detected without the tag, so we chose two complementary methods to evaluate whether the distribution changed. We conducted cryosectioning (no staining) on tumors injected with liposomes with and without REMNANT and 3D microscopy on tumors injected with gold nanoparticles with and without REMNANT. Cryosectioning allows both types of liposomes to be visualized. Blood vessels in the tumor were labeled with GSL1-Cy5 injected intravenously, and the liposome distribution was assessed against the blood vessels. We found that the distributions at the tissue level were indistinguishable between liposomes with and without REMNANT (Figure S3). We substituted gold nanoparticles for lipid nanoparticles to test the distribution using 3D microscopy. We used gold nanoparticles because they can be retained within tissues and visualized using their optical scattering in cleared tissues.[11−13] We conjugated gold nanoparticles with and without the tag (Table S2), processed the tissue using the tissue clearing technique, and analyzed whether the gold nanoparticles' distance away from blood vessels was different. We found that these distributions were not statistically different (Figure S4).

https://dx.doi.org/10.1021/acs.nanolett.9b04853
Nano Lett. 2020, 20, 1362−1369

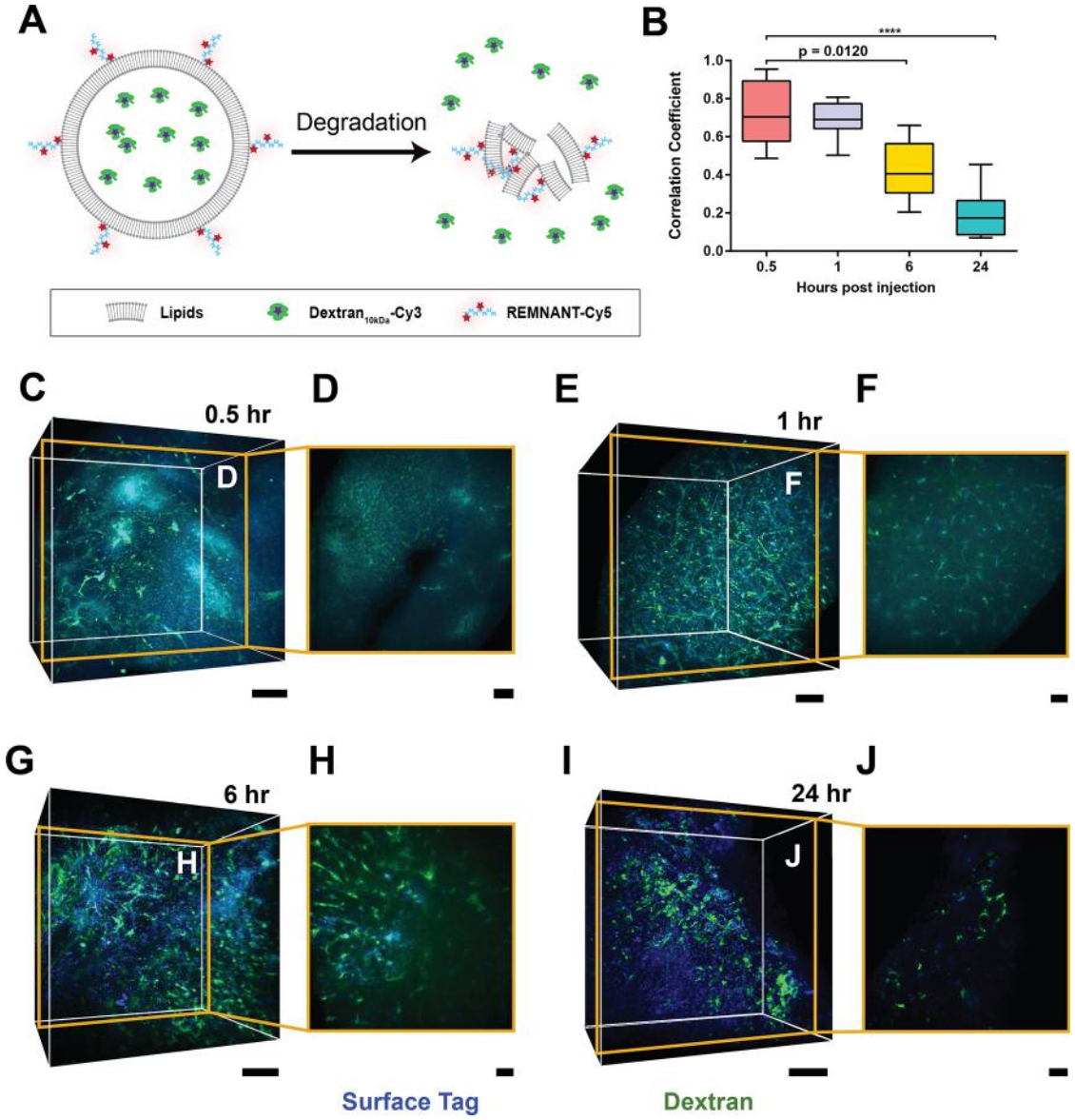

Figure 4. REMNANT allows visualization of liposome structural integrity in tissues. (A) Degradation scheme for dual-labeled liposome. (B) Correlation coefficient of internal (dextran-Cy3) and surface (K_7C−Cy5) tags of the liposome in the tumor over time. (C−J) Three-dimensional images and two-dimensional insets of dextran and liposome colocalization in a tumor slice across time points. For panel B, a box and whisker plot with n = 9−12 images acquired from 3 different animals. The center line indicates the median; box limits indicate upper and lower quartiles, and whiskers show the full range of values. The Kruskal−Wallis test followed by Dunn's correction for multiple comparisons was used to determine the P-values indicated. All P-values < 0.05 are indicated; **** indicates P < 0.0001. Scale bars indicate 200 μm for C, E, G, I and 100 μm for D, F, H, J.

We next explored whether REMNANT tags could be used to determine the structural integrity of liposomes inside tissues. Liposomes are commonly used as drug carriers with an encapsulated cargo that is released when the liposome loses its structural integrity. Fundamental understanding of liposome degradation in the tissue is critical to the design of drug carriers for optimal therapeutic effectiveness. Currently, researchers measure the stability of liposomes using *in vitro* assays, but these assays do not recapitulate the complexity of the *in vivo* environment because they lack the cells, tissue features, and circulation processes that influence the chemical processing and metabolism of lipids[21] (Figure S5). The structural integrity of liposomes in tissues is valuable for designing optimal therapeutics and understanding their mechanism of action. Using the REMNANT strategy, we observed the chemical degradation of liposomes in mouse tissues by independently labeling the lipid with one fluorescent dye (present on the surface of the liposome) and the cargo with another fluorescent dye (present in the core of the liposome). These two labels colocalize when the liposomes are intact and become uncorrelated when the liposomes are disrupted and cargo is released (Figure 4A). This tagging strategy allows for direct quantification and 3D imaging of the liposome's structural integrity formulation *in vivo*.

To test this experimentally, we synthesized these dual-tagged liposomes. The first tag (10 kDa Cy3-labeled aminated dextran encapsulated within the liposome) labels the cargo inside, and the second tag (REMNANT-Cy5 conjugated to azide functional lipids) labels the lipids on the surface (Figure 4A). These dual-tagged nanoparticles were injected intravenously into CD-1-nude mice with U87MG xenograft tumors at a dose of 1.00×10^{14} particles per animal and allowed to

https://dx.doi.org/10.1021/acs.nanolett.9b04853
Nano Lett. 2020, 20, 1362−1369

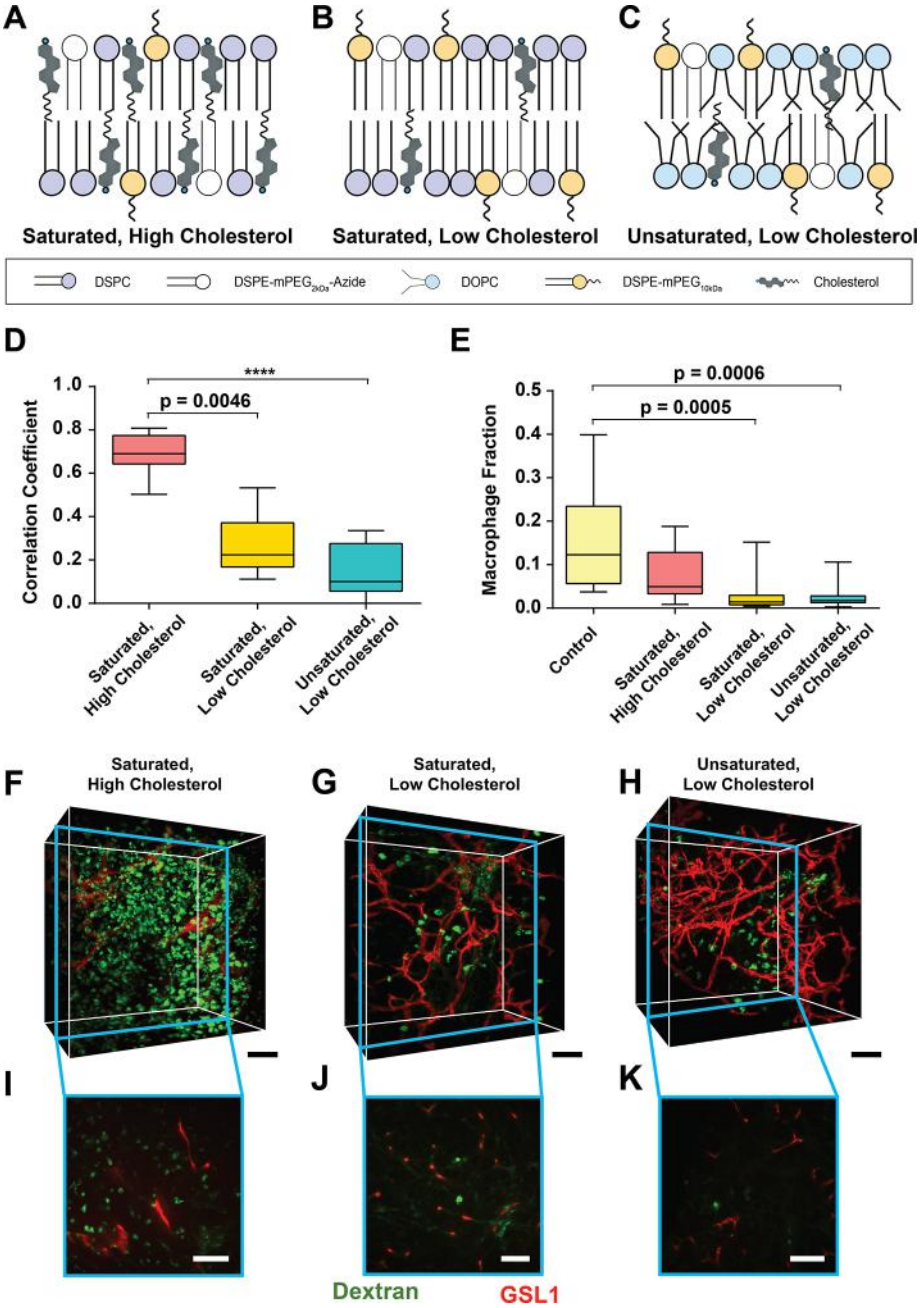

Figure 5. REMNANT allows visualization of liposome structural integrity in tissues. (A−C) Schematics of liposome designs with increasing degradation rates due to lower cholesterol content (10% compared to 40%) or replacement of saturated lipids with unsaturated lipids. (D) Correlation coefficient of internal (dextran-Cy3) and surface (K_7C−Cy5) tags of the liposome in the tumor over time for the three liposome designs. (E) Depletion of macrophages from the tumor quantified from 3D images due to the treatment of animals with clodronate encapsulated liposomes with lipid compositions shown in panels A−C. Control indicates tumors from animals injected with empty liposomes lacking clodronate. (F−H) Three-dimensional images of macrophage depletion in a tumor slice when treated with liposome designs containing clodronate. (F) was treated with saturated high cholesterol, (G) was treated with saturated low cholesterol, (H) was treated with unsaturated low cholesterol. (I-K) Zoomed in 2D slices taken from the 3D images shown in (F-H). For panels D and E, box and whisker plots display data with n = 9−12 images acquired from 3 different animals. The center line indicates the median; box limits indicate upper and lower quartiles, and whiskers show the full range of values. The Kruskal−Wallis test followed by Dunn's correction for multiple comparisons was used to determine the P-values indicated. All P-values <0.05 are indicated; **** indicates P < 0.0001. Scale bars indicate 100 μm.

circulate for 0.5, 1, 6, and 24 h post injection. Animals were sacrificed, and tumors were collected and cleared as previously described. We imaged cleared tumors using lightsheet microscopy in 3D and were able to detect both tags from these tissues. The cargo signal colocalized strongly with the surface signal at 0.5 and 1 h after injection but not at 6 and 24 h (Figure 4B−J). We quantified the colocalization of these signals by measuring the correlation coefficient between the two channels and found that the degree of colocalization decreased from 0.73 at 1 h postinjection, indicating high structural integrity to 0.43 and 0.20 at 6 and 24 h (Figure 4B), respectively. This is striking because we were unable to observe any degradation when we used the conventional *in vitro* serum incubation approach. We measured the leakage of the cargo tag

https://dx.doi.org/10.1021/acs.nanolett.9b04853
Nano Lett. 2020, 20, 1362−1369

over 168 h using *in vitro* serum incubation, but there was no statistical difference (Figure S5). These results suggest that liposome degradation takes place in the tissues rather than in serum and highlight the importance of measuring chemical parameters *in vivo* to improve the design of therapeutic nanoparticles.

To validate that internal and external liposome labels do not alter the pharmacokinetics and biodistribution of the liposomes, we synthesized three formulations of liposomes with DiR dye within the lipid membrane and varied the labeling strategy (liposomes DiR, liposomes DiR + cargo, and liposomes DiR + REMNANT). Blood was collected across a 24 h period to determine the pharmacokinetics, and organs were collected at 24 h to evaluate the biodistribution of the three liposomes formulations. Results showed similar pharmacokinetic profiles across 24 h (Figure S6), and there was no statistical difference between the liposome formulations across each respective organ (Figure S7). This suggests that REMNANT does not significantly affect the pharmacokinetics and biodistribution when attached on the surface of the liposome. However, we do recognize that the pharmacokinetics may change if the nanoparticle surface was significantly altered.

We examined whether the structural integrity and stability of liposomes would affect the therapeutic outcome in a mouse tumor model. We used clodronate as our therapeutic agent because it is a drug known to kill macrophages.[22] Unlike macrophages in the liver and spleen, macrophages in the tumor are associated with poor outcomes in a variety of tumor models and are the targets of treatment for multiple ongoing clinical trials.[23] Liposomes containing clodronate are capable of depleting macrophages in the liver, but their efficiency of depleting tumor-associated macrophages (TAMs) is unknown. This is because they are typically synthesized in the size range of 2−5 μm, which is too large to reach cells in the tumor, and the ideal release rates and structural composition are unknown. We synthesized 100 nm diameter liposomes because previous studies have suggested that this is an appropriate size to deliver therapeutics to tumors.[24] We also varied the cholesterol content and replaced saturated lipids with unsaturated lipids to manipulate the structural stability of liposomes. Saturated lipids have higher melting points than unsaturated lipids and increase the rigidity of the bilayer while cholesterol stabilizes the high surface curvature of the liposomes. We first tested the degradation of liposomes without clodronate using a tagged cargo and three membrane compositions: (design A) high cholesterol, fully saturated lipids, (design B) low cholesterol, fully saturated lipids, and (design C) low cholesterol, unsaturated lipids (Figure 5A−C, Videos S1−3, see Table S3 for full composition). We found that at 1 h postinjection, the colocalization coefficient decreased from 0.69 to 0.26 and 0.14 for design A, B, and C, respectively (Figure 5D). These results suggest that the three liposome compositions degraded at different rates *in vivo*. Additionally, we verified *in vitro* that liposome composition had no effect on the uptake in J744.1 macrophages, confirming degradation was the main cause of the decreasing signal colocalization (Figure S8).

Next, we encapsulated clodronate in these three compositions of liposomes to determine whether their therapeutic efficiency would change. We injected them intravenously into mice with U87MG tumors at a dose of 18 mg/kg of clodronate (Figures S9 and S10) and cleared the tissues as previously described. We imaged these tumors using 3D lightsheet microscopy and quantified the number of macrophages remaining in the tumor. We found that after 48 h, macrophages decreased from 15.0% of total cells without treatment to 7.3% for design A and 2.7% for designs B and C (Figure 5E−K). This shows that liposomes with low cholesterol and unsaturated lipids degraded faster and were more effective at depleting macrophages. We hypothesize that more effective depletion is due to their faster degradation, but we have not fully isolated all other confounding factors. This will be addressed in future studies.

More generally, our findings show that liposomes degrade >100-fold faster *in vivo* than *in vitro* (Figure 5D vs Figure S5). This finding is important to note because the rate of degradation affects the therapeutic outcome. Our chemical tag was key to discerning this finding. In the future, degradation rates could be measured to inform the design of liposomes so that their stability matches its penetration into the tumor core for maximized therapeutic response.

In conclusion, we developed a tag for 3D microscopy of lipid nanoparticles in tumors. Lipid nanoparticles are the most clinically successful nanoparticle formulation, but how they mechanistically deliver their payload to the tumors is not fully known. A method to better understand their delivery process in tumors is with 3D microscopy because we can better visualize their distribution in tumors. Our tag marks the location of liposomes in cleared tissues, which has not been possible before and allows us to examine both the distribution and degradation of these liposomes in intact tumors. The remaining challenge is optimizing the design of the tag to make it fully inert so that the same tag can be used to make both tissue-level and organ-level comparisons between different nanoparticle designs.

■ ASSOCIATED CONTENT

Supporting Information

The Supporting Information is available free of charge at https://pubs.acs.org/doi/10.1021/acs.nanolett.9b04853.

In vitro quantification of retention efficiency for different materials; 3D microscopy of PLGA nanoparticles in U87MG tumour using REMNANT; comparison of tissue distribution of nanoparticles with and without REMNANT; comparison of 3D distribution of nanoparticles with and without REMNANT; liposome release of cargo incubating in 90% mouse serum; pharmacokinetics of DiR liposomes to determine the effect of each component labels; biodistribution of DiR liposomes with different labeling strategies; *in vitro* macrophage uptake of different liposome designs; clodronate quantification using UPLC-MS; clodronate standard curve; hydrodynamic diameter and polydispersity index for organic nanoparticle designs; hydrodynamic diameter, polydispersity index and ζ potential of nanoparticle designs; lipid compositions for design A, B, and C; methods (PDF)

Video S1 (MP4)

Video S2 (MP4)

Video S3 (MP4)

■ AUTHOR INFORMATION

Corresponding Author

Warren C. W. Chan − *Institute of Biomaterials and Biomedical Engineering, Department of Chemistry, Chemical Engineering and Applied Chemistry, Terrence Donnelly Center for Cellular*

https://dx.doi.org/10.1021/acs.nanolett.9b04853
Nano Lett. 2020, 20, 1362−1369

and Biomolecular Research, and Materials Science and Engineering, University of Toronto, Toronto M5S 3G9, Canada; orcid.org/0000-0001-5435-4785; Phone: 416-946-0020; Email: warren.chan@utoronto.ca

Authors

Abdullah Muhammad Syed − *Institute of Biomaterials and Biomedical Engineering, University of Toronto, Toronto M5S 3G9, Canada;* orcid.org/0000-0001-9156-9662

Presley MacMillan − *Department of Chemistry, University of Toronto, Toronto M5S 3H6, Canada*

Jessica Ngai − *Institute of Biomaterials and Biomedical Engineering and Chemical Engineering and Applied Chemistry, University of Toronto, Toronto M5S 3G9, Canada*

Stefan Wilhelm − *Stephenson School of Biomedical Engineering, University of Oklahoma, Norman, Oklahoma 73072, United States;* orcid.org/0000-0003-2167-6221

Shrey Sindhwani − *Institute of Biomaterials and Biomedical Engineering, University of Toronto, Toronto M5S 3G9, Canada*

Benjamin R. Kingston − *Institute of Biomaterials and Biomedical Engineering, University of Toronto, Toronto M5S 3G9, Canada*

Jamie L. Y. Wu − *Institute of Biomaterials and Biomedical Engineering, University of Toronto, Toronto M5S 3G9, Canada*

Pablo Llano-Suárez − *Department of Physical and Analytical Chemistry, University of Oviedo, Oviedo 33006, Spain*

Zachary Pengju Lin − *Institute of Biomaterials and Biomedical Engineering, University of Toronto, Toronto M5S 3G9, Canada*

Ben Ouyang − *Institute of Biomaterials and Biomedical Engineering, University of Toronto, Toronto M5S 3G9, Canada*

Zaina Kahiel − *Department of Biochemistry, Microbiology, and Immunology, Faculty of Medicine, University of Ottawa, Ottawa K1N 6N5, Canada*

Suresh Gadde − *Department of Biochemistry, Microbiology, and Immunology, Faculty of Medicine, University of Ottawa, Ottawa K1N 6N5, Canada;* orcid.org/0000-0001-9102-3029

Complete contact information is available at:
https://pubs.acs.org/10.1021/acs.nanolett.9b04853

Author Contributions

○A.M.S., P.M., and J.N. contributed equally.

Notes

The authors declare no competing financial interest.

■ ACKNOWLEDGMENTS

We would like to acknowledge Anthony Tavares for ideas and discussions. We would also like to acknowledge the Canadian Research Chairs Program (950-223924), Canadian Cancer Society (502200 and 706286), Natural Sciences and Engineering Research Council (2015-06397 and graduate fellowships), Walter C. Sumner Memorial Fellowship (graduate fellowships), and Canadian Institute of Health Research (PJT-148848 and FDN-159932, and graduate fellowships) for funding support. We would also like to acknowledge the CFI facility. P.L. acknowledges funding support from the University of Oviedo (PAPI-18-PF-08).

■ REFERENCES

(1) Wilhelm, S.; Tavares, A. J.; Dai, Q.; Ohta, S.; Audet, J.; Dvorak, H. F.; Chan, W. C. W. Analysis of Nanoparticle Delivery to Tumours. *Nature Reviews Materials* **2016**, *1* (5), 16014.

(2) Park, K. Facing the Truth about Nanotechnology in Drug Delivery. *ACS Nano* **2013**, *7* (9), 7442−7447.

(3) Hare, J. I.; Lammers, T.; Ashford, M. B.; Puri, S.; Storm, G.; Barry, S. T. Challenges and Strategies in Anti-Cancer Nanomedicine Development: An Industry Perspective. *Adv. Drug Delivery Rev.* **2017**, *108*, 25−38.

(4) Jain, R. K.; Stylianopoulos, T. Delivering Nanomedicine to Solid Tumors. *Nat. Rev. Clin. Oncol.* **2010**, *7*, 653−664.

(5) Dai, Q.; Wilhelm, S.; Ding, D.; Syed, A. M.; Sindhwani, S.; Zhang, Y.; Chen, Y. Y.; MacMillan, P.; Chan, W. C. W. Quantifying the Ligand-Coated Nanoparticle Delivery to Cancer Cells in Solid Tumors. *ACS Nano* **2018**, *12* (8), 8423−8435.

(6) Chung, K.; Wallace, J.; Kim, S.-Y.; Kalyanasundaram, S.; Andalman, A. S.; Davidson, T. J.; Mirzabekov, J. J.; Zalocusky, K. A.; Mattis, J.; Denisin, A. K.; et al. Structural and Molecular Interrogation of Intact Biological Systems. *Nature* **2013**, *497* (7449), 332−337.

(7) Ertürk, A.; Becker, K.; Jährling, N.; Mauch, C. P.; Hojer, C. D.; Egen, J. G.; Hellal, F.; Bradke, F.; Sheng, M.; Dodt, H.-U. Three-Dimensional Imaging of Solvent-Cleared Organs Using 3DISCO. *Nat. Protoc.* **2012**, *7* (11), 1983−1995.

(8) Susaki, E. A.; Tainaka, K.; Perrin, D.; Yukinaga, H.; Kuno, A.; Ueda, H. R. Advanced CUBIC Protocols for Whole-Brain and Whole-Body Clearing and Imaging. *Nat. Protoc.* **2015**, *10* (11), 1709−1727.

(9) Hama, H.; Kurokawa, H.; Kawano, H.; Ando, R.; Shimogori, T.; Noda, H.; Fukami, K.; Sakaue-Sawano, A.; Miyawaki, A. Scale: A Chemical Approach for Fluorescence Imaging and Reconstruction of Transparent Mouse Brain. *Nat. Neurosci.* **2011**, *14* (11), 1481−1488.

(10) Eisenstein, M. Transparent Tissues Bring Cells into Focus for Microscopy. *Nature* **2018**, *564* (7734), 147−149.

(11) Sindhwani, S.; Syed, A. M.; Wilhelm, S.; Glancy, D. R.; Chen, Y. Y.; Dobosz, M.; Chan, W. C. W. Three-Dimensional Optical Mapping of Nanoparticle Distribution in Intact Tissues. *ACS Nano* **2016**, *10* (5), 5468−5478.

(12) Sindhwani, S.; Syed, A. M.; Wilhelm, S.; Chan, W. C. W. Exploring Passive Clearing for 3D Optical Imaging of Nanoparticles in Intact Tissues. *Bioconjugate Chem.* **2017**, *28* (1), 253−259.

(13) Syed, A. M.; Sindhwani, S.; Wilhelm, S.; Kingston, B. R.; Lee, D. S. W.; Gommerman, J. L.; Chan, W. C. W. Three-Dimensional Imaging of Transparent Tissues via Metal Nanoparticle Labeling. *J. Am. Chem. Soc.* **2017**, *139* (29), 9961−9971.

(14) Kingston, B. R.; Syed, A. M.; Ngai, J.; Sindhwani, S.; Chan, W. C. W. Assessing Micrometastases as a Target for Nanoparticles Using 3D Microscopy and Machine Learning. *Proc. Natl. Acad. Sci. U. S. A.* **2019**, *116*, 14937−14946.

(15) Barenholz, Y. (chezy). Doxil® — The First FDA-Approved Nano-Drug: Lessons Learned. *J. Controlled Release* **2012**, *160*, 117−134.

(16) Susaki, E. A.; Tainaka, K.; Perrin, D.; Kishino, F.; Tawara, T.; Watanabe, T. M.; Yokoyama, C.; Onoe, H.; Eguchi, M.; Yamaguchi, S.; et al. Whole-Brain Imaging with Single-Cell Resolution Using Chemical Cocktails and Computational Analysis. *Cell* **2014**, *157* (3), 726−739.

(17) Tainaka, K.; Kuno, A.; Kubota, S. I.; Murakami, T.; Ueda, H. R. Chemical Principles in Tissue Clearing and Staining Protocols for Whole-Body Cell Profiling. *Annu. Rev. Cell Dev. Biol.* **2016**, *32*, 713−741.

(18) Richardson, D. S.; Lichtman, J. W. Clarifying Tissue Clearing. *Cell* **2015**, *162* (2), 246−257.

(19) Matsumoto, K.; Mitani, T. T.; Horiguchi, S. A.; Kaneshiro, J.; Murakami, T. C.; Mano, T.; Fujishima, H.; Konno, A.; Watanabe, T. M.; Hirai, H.; et al. Advanced CUBIC Tissue Clearing for Whole-Organ Cell Profiling. *Nat. Protoc.* **2019**, *14*, 3506.

(20) Togami, K.; Daisho, T.; Yumita, Y.; Kitayama, A.; Tada, H.; Chono, S. Evaluation of Various Tissue-Clearing Techniques for the Three-Dimensional Visualization of Liposome Distribution in Mouse Lungs at the Alveolar Scale. *Int. J. Pharm.* **2019**, *562*, 218−227.

(21) Modi, S.; Anderson, B. D. Determination of Drug Release Kinetics from Nanoparticles: Overcoming Pitfalls of the Dynamic Dialysis Method. *Mol. Pharmaceutics* **2013**, *10* (8), 3076−3089.

(22) Buiting, A. M.; Van Rooijen, N. Liposome Mediated Depletion of Macrophages: An Approach for Fundamental Studies. *J. Drug Target.* **1994**, *2* (5), 357−362.
(23) Poh, A. R.; Ernst, M. Targeting Macrophages in Cancer: From Bench to Bedside. *Front. Oncol.* **2018**, *8*, 49.
(24) Uchiyama, K.; Nagayasu, A.; Yamagiwa, Y.; Nishida, T.; Harashima, H.; Kiwada, H. Effects of the Size and Fluidity of Liposomes on Their Accumulation in Tumors: A Presumption of Their Interaction with Tumors. *Int. J. Pharm.* **1995**, *121* (2), 195−203.

■ NOTE ADDED AFTER ASAP PUBLICATION

Due to a production error, this paper was published ASAP on January 22, 2020, with errors in the Abstract. The corrected version was reposted on January 23, 2020.

https://dx.doi.org/10.1021/acs.nanolett.9b04853
Nano Lett. 2020, 20, 1362−1369